Hindawi
Shock and Vibration
Volume 2019, Article ID 4532635, 14 pages
https://doi.org/10.1155/2019/4532635

Research Article

Disturbance Rejection in a One-Half Semiactive Vehicle Suspension by means of a *Fuzzy-H_∞* Controller

L. C. Félix-Herrán,[1] **Driss Mehdi**,[2] **José de Jesús Rodríguez-Ortiz**,[3] **Victor H. Benitez**,[4] **Ricardo A. Ramirez-Mendoza**,[3] **and Rogelio Soto**[3]

[1]*Tecnologico de Monterrey, School of Engineering and Sciences, Blvd. Enrique Mazón López 965, Hermosillo 83000, Sonora, Mexico*
[2]*LIAS-ENSIP, Université de Poitiers, Bât. B25, 2 Rue Pierre Brousse, Poitiers Cedex 86022, France*
[3]*Tecnologico de Monterrey, School of Engineering and Sciences, Ave. Eugenio Garza Sada 2501, Monterrey 64849, Nuevo Leon, Mexico*
[4]*Universidad de Sonora, Departamento de Ingeniería Industrial, Blvr. Luis Encinas y Rosales S/N, C.P. 83000, Col. Centro, Hermosillo, Sonora, Mexico*

Correspondence should be addressed to L. C. Félix-Herrán; lcfelix@tec.mx

Received 28 February 2019; Revised 15 June 2019; Accepted 1 July 2019; Published 31 July 2019

Academic Editor: Evgeny Petrov

A *fuzzy-H_∞* control, improved with weighting functions, has been designed and applied to a novel model of a one-half semiactive lateral vehicle (OHSLV) suspension. The herein contribution resides in the development and computation of an H_∞ controller with parallel distributed compensation (PDC) designed from a highly nonlinear system modelled via the Takagi–Sugeno (T-S) fuzzy approach. A *fuzzy-H_∞* controller is synthesized for an OHSLV T-S fuzzy model of a suspension with two magnetorheological (MR) dampers including actuators' nonlinear dynamics. The realism of results has been improved by considering the MR damper's behaviours (viscoplasticity, hysteresis, and saturation) and the handling of the phase angle of the sinusoidal disturbance, not included in other reported work. Time-domain tests remark transient time achievements, whereas precise performance criterion indices in the frequency domain are employed to assess the generated outcomes. The proposed solution complies with all performance criteria compared with a benchmark passive average suspension that fails in satisfying most of the performance criteria.

1. Introduction

Ground vehicle suspension systems provide a certain level of passenger comfort and vehicle stability by covering a set of basic functions such as supporting vehicle's weight, keeping tires in contact with the road, holding an optimal height of the vehicle, and isolating passengers against vibrations from road's disturbances, among others [1]. From the variety of available suspensions, semiactive solutions have proven their contribution to an acceptable level of simultaneous comfort and stability. Filled with electrorheological (ER) or magnetorheological (MR) fluids [2, 3], they can modify their viscosity from liquid to semisolid in less than ten milliseconds [4]. Due to the advantages with respect to ER dampers, this research employs MR dampers for the suspension [5, 6].

Considering that MR dampers have nonlinear phenomena such as saturation, hysteresis, and dynamics of a fluid going through an orifice [7], obtaining an accurate modelling becomes a critical task when applying them for vehicle suspensions. One of the most employed MR damper nonlinear representations is the Bouc–Wen model, which is handled in this research [4].

The baseline study in vehicle suspensions is the passive one-half vehicle suspension. The analysis on ride comfort and vehicle stability can be obtained through a half-vehicle model, where roll or pitch dynamics are added to the vertical motion [8]. If the focus of the study is to analyse the effect of

road irregularities, road bumps, and potholes on vehicle stability and passenger comfort, studies should include the pitch angle; however, if the aim is the vehicle's behaviour during road curves, the roll angle is the adequate option [9].

The rationale of this research is to improve the deficiencies exhibited by the passive suspension in the time domain and frequency domain, although working with semiactive suspensions increases the system's complexity. This study works with a semiactive vehicle suspension model that includes vertical and pitch dynamics through the so-called bicycle model, a four-degree-of-freedom (4-DOF) system also known as the suspension lateral model [10]. This representation merges both front wheels into a single front one, and both rear wheels in the same manner. The lateral model includes vertical motion of the concentrated front and rear wheels, along with pitch and vertical dynamics of the sprung mass, and it is portrayed in Figure 1.

In Figure 1, it is assumed that front and rear suspensions have the same characteristics, and the centre of mass is not exactly in the middle of the vehicle; thus, distances a and b, measured from the centre of gravity (COG), are different. Moreover, front m_{tf} and rear m_{tr} unsprung masses could be different as well. To analyse the pitch angle θ for the sprung mass m_s, a moment of inertia I_y with respect to horizontal and transversal axes is required. Furthermore, k_{sf} and k_{sr} represent the front and rear suspension springs' constants, respectively, whereas c_{sf} and c_{sr} are the dampers' constants. In addition, tires' stiffness is represented by k_{tf} and k_{tr}. All Z variables describe vertical displacements (Z_s, Z_{tf}, and Z_{tr} are related to the system's masses, whereas Z_{rf} and Z_{rr} illustrate disturbance inputs from the road profile).

The state of the art includes outstanding control proposals for 4-DOF one-half vehicle suspension with vertical and lateral dynamics. Pan and Fan [11] developed a variable universe fuzzy control system with variable damping and stiffness, whose results are compared against passive suspension and common fuzzy controller. Sun and Yang [12] developed an adaptive fuzzy PID controller for a 5-DOF suspension with good outcomes in the frequency domain. Adaptive controllers have been derived in their own research direction. Sun et al. [13] proposed an adaptive backstepping control strategy with parameter uncertainties, and their controller design considered actuator's nonlinearities. Sun et al. [14] introduced a fault-tolerant adaptive robust controller able to compensate parameter uncertainties and disturbances. Krauze and Kasprzyk [15] considered road profile information as a preview signal and designed an adaptive feedforward least-mean squares (LMS) algorithm for a semiactive suspension with a Bouc–Wen model and generated results in the frequency domain. Sun et al. [16] developed an adaptive vibration control strategy for nonlinear uncertain suspension and employed a hydraulic cylinder as the actuator. Another research line is state/output feedback and H_∞ controllers. Kong et al. [17] designed an H_∞-static output feedback controller (SOFC) based on particle swarm optimization (PSO) and differential evolution (DE) algorithms. Li et al. [18] applied multiobjective control to synthesize an H_∞/H_2 SOFC, whereas Suzuki et al. [19] reported a robust H_2 control to improve

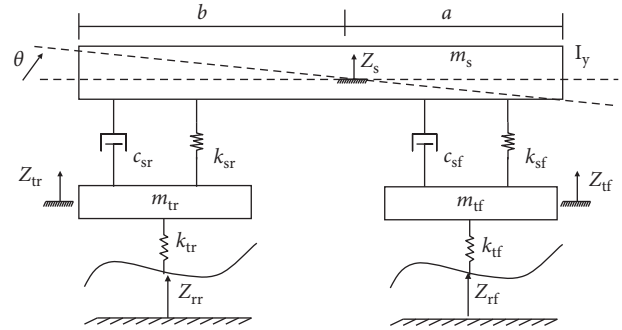

Figure 1: 4-DOF vehicle suspension system (bicycle model).

comfort and stability. Wang et al. [20] tested a SOFC based on variable substitution as an optimization algorithm to relax restriction during calculation of a feasible gain matrix.

More recent results have focused on semiactive suspensions with MR dampers. Krauze and Kasprzyk [21] employed the damper's Spencer model and developed a LQ state-feedback controller to improve two performance criteria in the frequency domain. Mahdi [22] designed an LQR-chaos control-oriented system based on an optimal Ott–Grebogi–Yorke approach with relevant results in the time domain. Wu and Liu [23] reported an MR semiactive system represented with a piecewise approximation model that modelled nonlinearities with a hyperbolic tangent function. Results were generated in the frequency domain. In addition, Pang et al. [24] developed a fuzzy controller for an experimental MR semiactive suspension based on neural networks and particle swarm optimization.

All these contributions are notable results in frequency and time domains, and their outcomes were compared against a passive or active benchmark suspension. Even though the state of the art provides important improvements in passenger comfort and vehicle stability, for the best of authors' knowledge, none of them individually reports a solution that considers actuator's nonlinear dynamics in controller computation, as well as time-domain and frequency-domain tests paired with performance indexes. Moreover, an opportunity area is the lack of study of the phase angle in the profile signal when it is analysed as a sinusoidal input.

This work considers the reported 4-DOF one-half vehicle suspension lateral model in the study of Félix-Herrán et al. [25] and the *fuzzy-*H_∞ controller for a one-quarter vehicle developed in the study of Félix-Herrán et al. [26], and it includes the disturbance phase angle and computes a *fuzzy-*H_∞ controller that complies with a set of performance criteria. This article is organized as follows: Section 2 states the performance criteria, and Section 3 provides a brief review of the control-oriented one-half suspension model applied herein. Section 4 reviews some peculiar aspects when employing sinusoidal signals as disturbances from road profile, Section 5 solves the *fuzzy-*H_∞ problem for the T-S nonlinear suspension, Section 6 presents the numerical case study and carries out a comparative analysis between the passive and the proposed semiactive solution. Finally, conclusions and brief information about further research

work complete the article in Section 7. It is out of the scope of this report to develop the MR damper's characteristics and to review the Takagi–Sugeno fuzzy model of a one-half semiactive vehicle suspension: lateral approach.

2. Performance Criteria

In automotive suspensions, the most important aspects to consider are passenger comfort and vehicle stability. The goal is to have a suspension system that meets both performance indices simultaneously, and therefore, these benchmarks must be considered during the controller design process. Before criteria are presented, it is important to give more information about passenger comfort and vehicle stability.

The comfort in this study refers to the performance index related to the vibrations generated from the road profile. These vibrations travel through the physical elements of the vehicle and are transmitted to passengers, causing annoyance when vibrations are inside a range of frequencies (human body resonant frequencies are around 5 Hz [27] and exceed certain specified amplitude values). For example, human dizziness and motion sickness are stronger around 1 Hz. Even though passenger comfort level is very subjective (persons are different regarding their physical aspects such as anthropological and sensorial capacities), it is necessary to come up with a standard to measure passenger comfort.

Vehicle stability is related to steering wheel changes and disturbances from the environment, e.g., road profile irregularities. In this research, stability is focused on the suspension's ability to keep the tires in contact with the road surface against external disturbances (the road profile) [28].

2.1. Time Domain. The objective is to keep all the variables of interest inside the physical limits and to reduce, as much as possible, the overshoot and the settling time of chassis displacement, tire displacement, chassis acceleration, suspension deflection, pitch angle, and pitch acceleration when compared with a passive suspension [29–33].

2.2. Frequency Domain. The focus is to evaluate vertical and pitch suspension performances of average city vehicles in terms of some frequency-domain indices. Accepted input signals for these tests are $Z_r = 0.015 \sin \omega t(m)$ for low frequencies and $Z_r = 0.001 \sin \omega t(m)$ for high frequencies [28–30]. The benchmarks are described below:

(1) Passenger comfort at low frequencies (0–4 Hz): limit the relation (gain) *chassis displacement/road profile* to be less than 2.0, nearby the sprung mass resonance frequency for an average city vehicle, i.e., 1.1 Hz.

(2) Road holding (0–15 Hz): limit the relation (gain) *tire displacement/road profile* to be less than 1.8, around the sprung mass resonance frequency, i.e., approximately 10 Hz for a compact city vehicle.

(3) Passenger's comfort at high frequencies (4–30 Hz): maintain chassis rms (root-mean- square) acceleration below the limits reported in the study of Wong [28] to ensure a passenger comfort condition for 8 hours.

(4) Suspension travel (deflection) within physical limits (0–4 Hz): this is a restriction that must be considered when evaluating vehicle suspensions. Deflection must always remain within the damper's physical limits to increase its useful life and avoid nonmodelled dynamics when limits are reached.

(5) To the best of authors' knowledge, no specific criterion related to θ has been found in reported work. The aim in this inquiry is to decrease the pitch angle θ, as much as possible, between 0 and 4 Hz, compared against a reference passive suspension, as in [31].

(6) Wong [28] displayed a benchmark proposed by the ISO (International Organization of Standardization). The criterion illustrates the maximum allowable rms chassis pitch angle acceleration within a frequency range of interest. Like rms vertical chassis acceleration, the author provides curves that bound the maximum value to ensure passenger comfort during certain time. The goal is to have 8 hours of passenger comfort for pitch acceleration.

Because the performance criteria for vertical and pitch acceleration are expressed in m/s^2 and the generated herein results are presented in rad/s^2, it is required to have an equation to relate both units. To develop this idea, D'Souza and Gang [34] dealt with equations that measure the moment of inertia I for a set of different solids rotating with respect to an arbitrary axis. Considering a bicycle model vehicle's sprung mass, m_s, is viewed as a cylinder of radius r that rotates around a pitch axis y, the following equation holds:

$$I_y = \frac{1}{2} m_s r^2. \tag{1}$$

From equation (1), r can be expressed as follows:

$$r = \sqrt{\frac{2I_y}{m_s}}, \tag{2}$$

where I_y has previously been defined for the sprung mass. Thus, with the calculated r, angular acceleration $\ddot{\theta}$ is converted into a linear acceleration as presented below:

$$\ddot{\theta}\left(\mathrm{m/s^2}\right) = \ddot{\theta}\left(\mathrm{rad/s^2}\right) r\,(\mathrm{m}). \tag{3}$$

3. One-Half Semiactive Suspension Model

The passive dampers have been replaced by magnetorheological elements to achieve different damping forces in real time. The target system is a 4-DOF one-half suspension with two MR dampers, as in Figure 2. Dynamic equations and some other basic aspects of a general bicycle model are developed by Rajamani [35].

From Figure 2, the following state variables were defined: $x_1 = Z_s$, $x_2 = \dot{Z}_s$, $x_3 = \theta$, $x_4 = \dot{\theta}$, $x_5 = Z_{tf}$, $x_6 = \dot{Z}_{tf}$, $x_7 = Z_{tr}$, $x_8 = \dot{Z}_{tr}$, $x_9 = z_{MRf}$, and $x_{10} = z_{MRr}$; $u_1 = i_f$ and $u_2 = i_r$; and

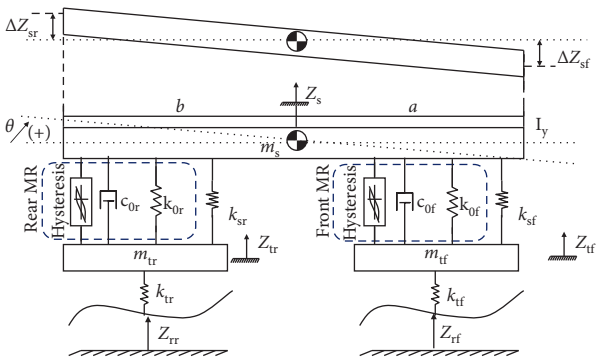

Figure 2: A 4-DOF one-half semiactive suspension.

$w_1 = Z_{rf}$ and $w_2 = Z_{rr}$. The suspension system is defined in the following equations:

$$\dot{x}_1 = x_2, \tag{4}$$

$$\begin{aligned} m_s\dot{x}_2 = {} & -(K_1 + K_2)x_1 - (c_{0fa} + c_{0ra})x_2 + (a-b)(K_1)x_3 \\ & + (a-b)c_{0fa}x_4 + (K_1)x_5 + c_{0fa}x_6 + (K_2)x_7 + c_{0ra}x_8 \\ & - \alpha_f x_9 - \alpha_r x_{10} + Z_1 u_1 + Z_2 u_2, \end{aligned} \tag{5}$$

$$\dot{x}_3 = x_4, \tag{6}$$

$$\begin{aligned} I_y\dot{x}_4 = {} & (aK_1 - bK_2)x_1 + (ac_{0fa} - bc_{0ra})x_2 \\ & - \left[a^2K_1 + b^2K_2\right]x_3 - \left(a^2c_{0fa} + b^2c_{0ra}\right)x_4 - aK_1x_5 \\ & - ac_{0fa}x_6 + bK_2x_7 + bc_{0ra}x_8 + a\alpha_{fa}x_9 - b\alpha_{ra}x_{10} \\ & - aZ_1u_1 + bZ_2u_2, \end{aligned} \tag{7}$$

$$\dot{x}_5 = x_6, \tag{8}$$

$$\begin{aligned} m_{tf}\dot{x}_6 = {} & K_1x_1 + c_{0fa}x_2 - aK_1x_3 - ac_{0fa}x_4 - K_3x_5 - c_{0fa}x_6 \\ & + \alpha_{fa}x_9 + k_{tf}w_1 - Z_1u_1, \end{aligned} \tag{9}$$

$$\dot{x}_7 = x_8, \tag{10}$$

$$\begin{aligned} m_{tr}\dot{x}_8 = {} & K_2x_1 + c_{0ra}x_2 + bK_2x_3 + bc_{0ra}x_4 - K_3x_7 - c_{0ra}x_8 \\ & + \alpha_{ra}x_{10} + k_{tr}w_2 - Z_2u_2, \end{aligned} \tag{11}$$

$$\dot{x}_9 = Z_3x_9 + \delta_f x_2 - a\delta_f x_4 - \delta_f x_6, \tag{12}$$

$$\dot{x}_{10} = Z_4x_{10} + \delta_r x_2 + b\delta_r x_4 - \delta_r x_8, \tag{13}$$

where $K_1 = k_{sf} + k_{0fa}$, $K_2 = k_{sr} + k_{0ra}$, and $K_3 = k_{sf} + k_{0fa} + k_{tf}$.

The proposed OHSLV system contains two MR dampers, and each damper provides two nonlinearities to the whole system. As a result, Z_1 to Z_4 are the four nonlinear terms to model, and they are defined in the following equations:

$$\begin{aligned} Z_1 = {} & -k_{0fb}x_1 - c_{0fb}x_2 + ak_{0fb}x_3 + ac_{0fb}x_4 + k_{0fb}x_5 \\ & + c_{0fb}x_6 - \alpha_{fb}x_9, \end{aligned} \tag{14}$$

$$\begin{aligned} Z_2 = {} & -k_{0rb}x_1 - c_{0rb}x_2 - bk_{0rb}x_3 - bc_{0rb}x_4 + k_{0rb}x_7 \\ & + c_{0rb}x_8 - \alpha_{rb}x_{10}, \end{aligned} \tag{15}$$

$$Z_3 = -\left[\gamma_f\left|x_2 - ax_4 - x_6\right| + \beta_f(x_2 - ax_4 - x_6)\operatorname{sgn}(x_9)\right]|x_9|, \tag{16}$$

$$Z_4 = -\left[\gamma_r\left|x_2 + bx_4 - x_8\right| + \beta_r(x_2 + bx_4 - x_8)\operatorname{sgn}(x_{10})\right]|x_{10}|, \tag{17}$$

where $\beta_f = \beta_r$, $\gamma_f = \gamma_r$, and $\delta_f = \delta_r$. In addition, $\operatorname{sgn}(x_9)$ and $\operatorname{sgn}(x_{10})$ are defined by

$$|\zeta| = \zeta \operatorname{sgn}(\zeta), \tag{18}$$

where $\operatorname{sgn}(\zeta)$ is equal to -1 if $\zeta < 0$, 0 if $\zeta = 0$, and $+1$ if $\zeta > 0$. Explained in the study of Tanaka and Wang [36], 2^n linear subsystems are generated from n nonlinearities. Hence, Z_1 to Z_4 are replaced with 16 linear subsystems interconnected with fuzzy membership functions (M_1, M_2, N_1, N_2, P_1, P_2, Q_1, and Q_2) and linking functions (h_1 to h_{16}). The whole system is fully expressed with the following Takagi–Sugeno fuzzy model where each nonlinear term was represented by two linear systems interconnected via fuzzy membership functions. Further explanations about the MR damper's composition and its behaviour are extensively explained in [4], whereas the complete development of the half-vehicle semiactive suspension model with the MR dampers is found in [25]:

$$\dot{x}(t) = \sum_{i=1}^{16} h_i\left[A_i x(t) + B_i u(t)\right] + B_w w(t), \tag{19}$$

$$z(t) = C_z x(t) + D_u u(t) + D_w w(t), \tag{20}$$

where $x(t)$ is the state vector, $u(t)$ represents the command input, and $w(t)$ is the disturbance signal coming from the road profile. Subindex i refers to the i-th linear subsystem, whereas $z(t)$ is the controlled output vector that complies with previously stated performance criteria.

For further control purposes, the state vector $x(t)$ contains all relevant system's state variables, and it is defined as $\left[Z_s\ \dot{Z}_s\ \theta\ \dot{\theta}\ Z_{tf}\ \dot{Z}_{tf}\ Z_{tr}\ \dot{Z}_{tr}\ z_{MR}\ z_{MRr}\right]^T$ and associated with A_i, whereas the command input vector $[i_f\ i_r]^T$ is related to B_i, and the disturbance input vector $[Z_{rf}\ Z_{rr}]^T$ is linked to B_w.

4. Considering a Realistic Scenario

When working with a one-half vehicle suspension model, an important aspect is the disturbance input phase angle. The 4-DOF one-half vehicle suspension has two external inputs coming from the road profile (Z_{rf} and Z_{rr}). It could be assumed that in real life, sinusoidal signals representing irregular surfaces have the same amplitude and frequency, but the phase angle among them is different. This is due to

vehicle's length, translational velocity, and uneven road profiles.

The authors of this study consider that phase angle φ must be included in simulation work to consider real conditions. Ignoring angle φ or if both tires are always in phase is unrealistic. For example, Figure 3 portrays a vehicle moving with translational velocity v. Signals Z_{rf} and Z_{rr} are always in phase, which means that φ is always zero; seldom true in real suspension systems. Two unrealistic scenarios are illustrated (both disturbances are exactly on top of the sinusoidal signal, or both at the bottom).

A more realistic scenario is depicted in Figure 4, where φ is not zero, i.e., Z_{rf} and Z_{rr} are not in phase.

To estimate phase angle φ some calculations must be performed from previous knowledge of v (translational velocity), f (frequency), and distances a and b. Velocity v, usually expressed in km/hr, must be translated into m/s, by

$$v\,(\text{m/s}) = \frac{v\,(\text{km/hr})}{3.6}. \tag{21}$$

Moreover, the wavelength λ of a sinusoidal wave can be defined as the spatial period of the wave, i.e., the distance over the wave, before the pattern repeats itself [37]:

$$v = \frac{\lambda}{T} = \lambda f, \tag{22}$$

where f is the wave's frequency, i.e., number of instances per unit time of a repeating event, whereas T is the signal's period; that is, the duration of one cycle in a repeating event [38]. In equation (22), λ is defined as follows:

$$\lambda = \frac{v}{f}\,(\text{m/cycle}). \tag{23}$$

In Figure 5, it can be noted that $(a+b)/\lambda$ generates an integer when Z_{rf} and Z_{rr} are in phase; however, as mentioned before, this is an occasional situation. The generic relation between vehicle length $(a+b)$ and wavelength λ is given as follows:

$$E + F\,(\text{cycle}) = \frac{(a+b)}{\lambda}, \tag{24}$$

where E is an integer and F is a fraction that represents the phase angle φ, as in Figure 5. Equation (24) is the baseline to obtain F:

$$F = \frac{(a+b)}{\lambda} - E\,(\text{cycle}), \tag{25}$$

where F is a fraction of one entire cycle of the wave, and it is closely related to the phase angle φ. For that reason, F has a value between 0 and 2π (radians). From equation (25), φ could be measured in degrees and radians as presented in the following equations:

$$\varphi = 360F\,(\text{degrees}), \tag{26}$$

$$\varphi = 2\pi F\,(\text{radians}). \tag{27}$$

In Figure 5, the vehicle length $a+b$ is constant, and the graphical magnitude of φ is measured from the rear dot

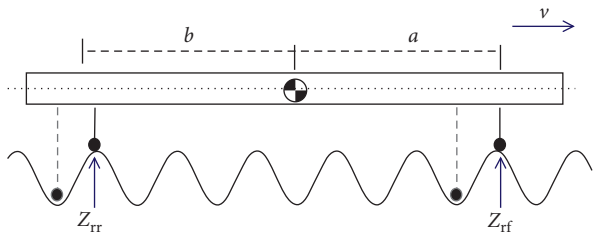

Figure 3: Disturbance inputs Z_{rf} and Z_{rr}. Both cases scarcely happen.

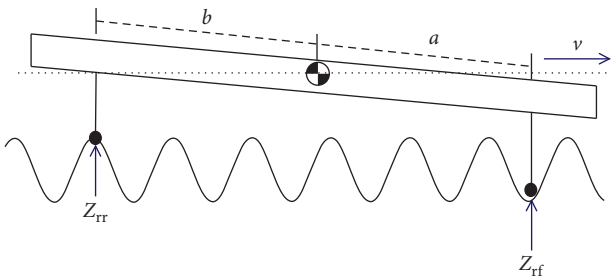

Figure 4: Disturbance inputs Z_{rf} and Z_{rr}. Phase angle φ is not zero.

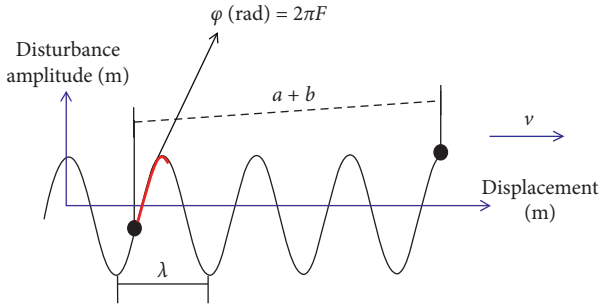

Figure 5: Phase angle φ and its relation to F.

closest to the amplitude axis, to the wave's peak. The herein simulation work calculated φ for each frequency applied value and included it in the input signal, a disturbance coming from the road profile. To the best of authors' knowledge, this phase angle φ consideration for road profile inputs Z_{rf} and Z_{rr} has not been reported yet.

5. Controller Design

For this research, control design effort focused on stability and frequency-domain performance via a *fuzzy-H_∞* controller. Even though the first approach in control design was a static state feedback controller (SSFC) to guarantee stability in closed loop, there were not enough degrees of freedom to design based on performance criteria; hence, a *fuzzy-H_∞* controller became an attractive option (the closed-loop diagram is presented in Figure 6).

5.1. Fuzzy-H_∞ Controller to Achieve Stated Performance Criteria in Frequency Domain. The nonlinear one-half suspension model is a set of linear subsystems interconnected via fuzzy

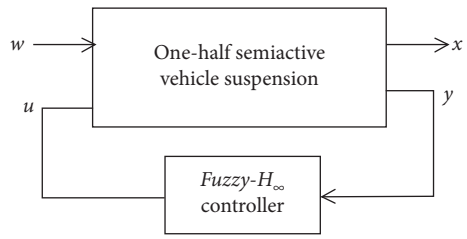

Figure 6: Semiactive suspension system (disturbance rejection).

membership functions [25]. The applied closed loop is as follows.

For the OHSLV, each T-S model's linear subsystem can be represented by a linear time-invariant (LTI) system, as defined in equations (19) and (20). The applied control approach referred to the H_∞ norm stated as

$$\left\|T_{zw}\right\|_\infty = \sup_w \sigma\left|T_{zw}(jw)\right|, \tag{28}$$

where the right part of the equation represents the largest singular value σ for the transfer function T_{zw}, which is the ratio (controlled output z/input disturbance w) along a frequency range. It is important to mention that an H_∞ approach seeks to keep T_{zw} norm below a target value, along a frequency of interest. In this research, the H_∞ controller aims to obtain a fuzzy controller that guarantees stability as well as a closed loop system with a γ disturbance rejection level. The general formulation has been reported in the study of Assawinchaichote et al. [39] and presented in the form of linear matrix inequalities [40] as in the following equations:

$$\begin{bmatrix} A_iP + PA_i^T + B_iY_j + Y_j^TB_i^T & B_w & PC_z^T + Y_j^TD_u^T \\ B_w^T & -\gamma^2 I & D_w^T \\ C_zP + D_uY_j & D_w & -I \end{bmatrix} < 0, \quad \forall i, j = 1, 2, \ldots, N, \tag{29}$$

$$P = P^T > 0, \tag{30}$$

where N is the number of subsystems, $\gamma > 0$, and

$$K_j = Y_jP^{-1}. \tag{31}$$

Individual controller gains K_j were calculated for each linear subsystem in the one-half vehicle suspension. Moreover, the total fuzzy control law was composed through parallel distributed compensation (PDC) [36, 41]:

$$u(t) = \sum_i^N h_i(t)K_ix(t), \tag{32}$$

where the set of $h_i(t)$ must comply with

$$0 \le h_i \le 1, \qquad \sum_{i=1}^N h_i = 1. \tag{33}$$

For the system defined in equations (19) and (20), the controller synthesis employed matrices C_z, D_u, and D_w as follows:

$$C_z = \begin{bmatrix} 1 & 0 & 0 & 0 & 0 & 0 & 0 & 0 & 0 & 0 \\ 0 & 0 & 0 & 0 & 1 & 0 & 0 & 0 & 0 & 0 \\ 0 & 0 & 0 & 0 & 0 & 0 & 1 & 0 & 0 & 0 \end{bmatrix}, \tag{34}$$

$$D_u = D_w = \begin{bmatrix} 0 & 0 \\ 0 & 0 \\ 0 & 0 \end{bmatrix}. \tag{35}$$

The proposed equations (34) and (35) adhere to the state, command input, and disturbance input vectors described at the end of Section 3. An analysis on equation (34) remarks that the *fuzzy-H_∞* approach impacts on the unsprung mass displacement and on the front and rear tires' displacements.

5.2. Modification to the Control Strategy via Weighting Functions. This work applied weighting functions [42] in the controller gains' computation to improve the control outcomes. According to Son et al. [43], a valid weighting function must be stable, rational, and represented with minimum phase transfer function, i.e., all poles and zeros must be in the half left plane of the so-called S plane.

To improve comfort and stability performance, three weighting functions were added to control synthesis in equation (29). For low-frequency performance, i.e., 0.5–4 Hz, a high-pass filter was included. For high-frequency enhancement (beyond 7 Hz), two low-pass filters, one per unsprung mass, were considered in the controller's calculation. These weighting functions (W_f) of affine transfer functions changed the norm definition in equation (28) to be as follows:

$$\left\|T_{zw}W_f\right\|_\infty = \sup_w \sigma\left|T_{zw}W_f(jw)\right|. \tag{36}$$

The modified system was verified for stability and detectability [44]. It is important to highlight that weighting functions were incorporated to obtain a controller; i.e., it is only for the controller design. The next step is to define the structure and numerical values for W_f. For this research context, one-half suspension corresponds to a city vehicle with sprung mass resonant frequency between 1.1 and 1.5 Hz, whereas unsprung masses hold resonant frequencies in a range of 2.3 to 3 Hz. [35]. The second resonant peak for tire displacement is near 10 Hz. With this information, two first-order high-pass filters, with similar cutoff frequency, were proposed, and their transfer function is defined as follows:

$$\text{Gfilter}_{\text{highpass}}(s) = \frac{s}{s + w_{c1}}, \tag{37}$$

where $w_{c1} = 2\pi f_{c1}$, and the first order low-pass filter has the following transfer function:

$$\text{Gfilter}_{\text{lowpass}}(s) = \frac{w_{c2}}{s + w_{c2}}, \tag{38}$$

where $w_{c2} = 2\pi f_{c2}$. The corner-frequency numerical values f_{c1} and f_{c2} are presented and explained in Section 6. In addition, equations (37) and (38) are transformed into the state-space domain to achieve the following equations:

$$A_f = \begin{bmatrix} A_{fs} & 0 & 0 \\ 0 & A_{fu1} & 0 \\ 0 & 0 & A_{fu2} \end{bmatrix}, \quad (39)$$

$$B_f = \begin{bmatrix} B_{fs} & 0 & 0 \\ 0 & B_{fu1} & 0 \\ 0 & 0 & B_{fu2} \end{bmatrix}, \quad (40)$$

$$C_f = \begin{bmatrix} C_{fs} & 0 & 0 \\ 0 & C_{fu1} & 0 \\ 0 & 0 & C_{fu2} \end{bmatrix}, \quad (41)$$

$$D_f = \begin{bmatrix} D_{fs} & 0 & 0 \\ 0 & D_{fu1} & 0 \\ 0 & 0 & D_{fu2} \end{bmatrix}, \quad (42)$$

where f_s stands for the filter-sprung mass, fu1 refers to filter-unsprung mass 1, and fu2 symbolizes filter-unsprung mass 2. The augmented system is represented as follows:

$$\begin{bmatrix} \dot{x} \\ \dot{x}_f \end{bmatrix} = \begin{bmatrix} A & 0 \\ B_f C & A_f \end{bmatrix} \begin{bmatrix} x \\ x_f \end{bmatrix} + \begin{bmatrix} B_u \\ B_f D_u \end{bmatrix} u + \begin{bmatrix} B_w \\ B_f D_w \end{bmatrix} w, \quad (43)$$

$$z_f = \begin{bmatrix} D_f C & C_f \end{bmatrix} \begin{bmatrix} x \\ x_f \end{bmatrix} + \begin{bmatrix} D_f & D_u \end{bmatrix} u + \begin{bmatrix} D_f & D_w \end{bmatrix} w, \quad (44)$$

where the desired output vector z_f should comply with the performance criteria in Section 2. Equations (43) and (44) hold for each linear subsystem of the T-S fuzzy model.

5.3. Ill-Conditioned Matrices and LMI-Controller Computation. It is widely known that a system in the state space can be represented in many ways without altering the system's eigenvalues and that this representation has an impact on controller calculation [45]. Although from one realization to another one, the state, input, and output matrices have different numerical values, the eigenvalues do not change, and overall behaviour remains the same. Furthermore, the eigenvectors are different among representations, but they are related by means of a transformation matrix. A general transformation matrix T is defined in the following equation:

$$\dot{x}_t = Tx(t), \quad (45)$$

where $\dot{x}_t$ stands for the modified $\dot{x}$ and the state-space realization is as follows:

$$\begin{aligned} \dot{x}_t &= TAT^{-1}x(t) + TBu(t), \\ z_t(t) &= CT^{-1}x(t) + Du(t). \end{aligned} \quad (46)$$

For the target system in equations (43) and (44), the transformation matrix T generated the following representation:

$$\begin{aligned} \begin{bmatrix} \dot{x} \\ \dot{x}_f \end{bmatrix}_t &= T \begin{bmatrix} A & 0 \\ B_f C & A_f \end{bmatrix} T^{-1} \begin{bmatrix} x(t) \\ x_f(t) \end{bmatrix} + T \begin{bmatrix} B_u \\ B_f D_u \end{bmatrix} u(t) \\ &\quad + T \begin{bmatrix} B_w \\ B_f D_w \end{bmatrix} w(t), \end{aligned} \quad (47)$$

$$z_t(t) = \begin{bmatrix} D_f C \end{bmatrix} T^{-1} \begin{bmatrix} x(t) \\ x_f(t) \end{bmatrix} + \begin{bmatrix} D_f D_u \end{bmatrix} u(t) + \begin{bmatrix} D_f D_w \end{bmatrix} w(t). \quad (48)$$

When solving a set of LMIs in MATLAB, the convergence to a solution depends on the state-space realization [40]. In this study, during the computation process of K_j, it was observed that the calculated gains were very small and a hypothesis was stated. Due to the matrix ill conditioning (directly generated from the fuzzy T-S representation), it was difficult to calculate a set of K_j that fulfilled the feasibility problem for solving all the LMIs. Authors tested different state-space representations and through the modal canonical transformation [46], larger values of K_j were computed to generate a more significant command vector $[i_f\ i_r]^T$. The exploration of different state-space representations to solve the LMIs was an important part in the design and computation of the feedback gains.

Due to the transformation, a modified gain K_t to work for a modified vector xt was calculated. However, after the gain was computed, the T-S fuzzy model was left aside, and the controller was applied to the original nonlinear differential equations system; therefore, the controller gains must be returned to the original system's coordinates as follows:

$$K = K_t T. \quad (49)$$

In a T-S fuzzy model constituted by a set of linear subsystems, several controller gains K_i are going to be obtained and equation (49) is employed as follows:

$$K_i = K_{ti} T, \quad \text{for } i = 1, 2, \ldots, N, \quad (50)$$

where K_{ti} is the computed gain K_i for the transformed linear subsystem and T is the transformation matrix.

6. Case Study

Simulation results based on real data support the theoretical work in previous sections. The MR damper Bouc–Wen model numerical data were taken from a realistic damper's characterization [47], whereas the rest of parameters were adopted from [25]. MR dampers do not respond instantaneously to current changes; they are modelled as first-order systems with a time constant $\eta = 0.052$ ms [4]. The herein research employs a damper's maximum extension of 2.5 cm. In addition, front and rear suspensions and tire stiffnesses are the same, and dampers c_{sf} and c_{sr} are the referenced damping values (passive case). Furthermore, the centre of gravity is not in the middle of the vehicle's length;

thus, a is different from b. It is worthwhile to remember that distances a and b are measured from the vehicle's COG to the point where the chassis is in contact with the front and rear suspensions, respectively. Time-domain and frequency-domain tests consider the realistic scenario about the phase angle between Z_{rf} and Z_{rr}, as explained in Section 4. Table 1 lists all numerical values employed in the simulation work.

For the weighting functions, the cutoff frequencies f_c were chosen based on the suspension's resonance peaks and finely tuned to trial and error. One high-pass filter with $f_{c1} = 5.5$ Hz and two low-pass filters with $f_{c2} = f_{c3} = 2.3$ Hz were selected to decrease the suspension's resonant peaks. This information was considered during the *fuzzy-H_∞* controller synthesis.

Based on equations (47) and (48) and considering the baseline *fuzzy-H_∞* LMI formulation in equations (29) and (30), the controller's gains were calculated. The goal was to minimize the target variables contained in equation (44). It is relevant to remark that even though the ill-conditioning matrix behaviour was reduced with the applied system's transformation, the best computed value for γ was equal to 4.0; i.e., this was the smallest γ value that satisfied feasibility LMI problem programmed in MATLAB.

All the simulation work was carried out in MATLAB Simulink. From the MATLAB workspace, the values of the constants were loaded, and the tests were executed in time and frequency domains with the suspension systems developed in Simulink. Figure 7 presents the block diagram about the one-half semiactive suspension system with the *fuzzy-H_∞* controller.

6.1. Time-Domain Tests. This test refers to the system's response when the disturbance is a road bump-like signal of 4.0 cm high. To describe this behaviour, a cosine function like an inverted bell was employed to represent the road bump, as explained in [32], also applied in [48]. The disturbance is described in equations (51) and (52), also depicted in Figure 8:

$$\frac{dZ_{rf}}{dt} = 0.04\,(1 - \cos 8\pi t), \quad 0.5 \le t \le 0.75\,(\text{s}), \tag{51}$$

$$\frac{dZ_{rf}}{dt} = 0.04\,(1 - \cos 8\pi t), \quad 0.5 \le t \le 0.75\,(\text{s}). \tag{52}$$

Another important issue about the disturbance is that the road bump excites the front tire, and after some time, it affects the rear tire. The time between the front and rear wheels depends on the distance $(a + b)$ as well as the vehicle's forward velocity, v. The road bump signal seeks to comply with the realistic disturbance scenario explained in Section 4; thus, the simulation effort computed φ for each frequency testing value and included it in the input signal.

Time-domain suspension responses are depicted in Figures 9–16. The performance of the *fuzzy-H_∞* controller is compared against a passive suspension system with $c = 1{,}000$ Ns/m. Simulation time considers $0 \le t \le 4$ s; the required time to measure the variables of interest.

Table 1: One-half vehicle suspension parameters for simulation work.

Parameter	Value
m_s	800 kg
I_y	1,400 kg/m^2
a	1.38 m
b	1.36 m
$m_{tf} = m_{tr}$	40 kg
$k_{sf} = k_{sr}$	20,000 N/m
$k_{tf} = k_{tr}$	210,000 N/m
$c_{sf} = c_{rf}$	1,000 Ns/m
β	1.0×10^6 m^{-2}
γ	1.2×10^6 m^{-2}
δ	15

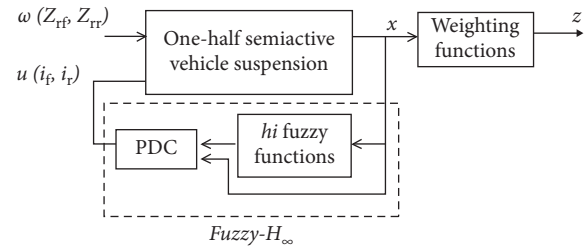

Figure 7: Semiactive suspension with a *fuzzy-H_∞* controller.

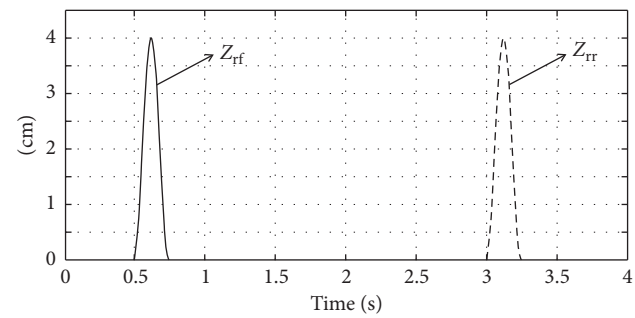

Figure 8: Road bump disturbance.

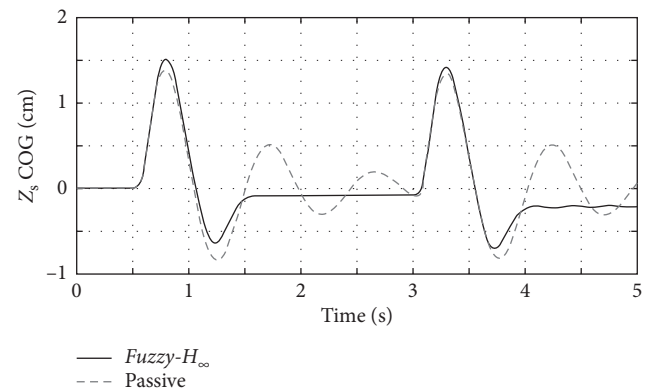

Figure 9: COG chassis displacement.

Table 2 extracts the key variables from Figures 9–16 to compare suspensions' performance via 16 criteria. *M*p stands for the maximum value in cm for Z_s and suspension

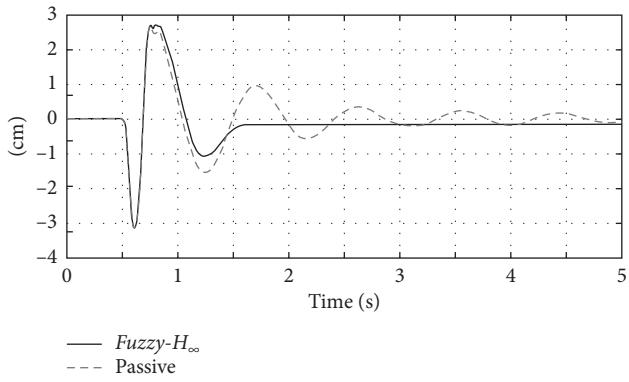

Figure 10: Front suspension's deflection ($Z_{sf} - Z_{tf}$).

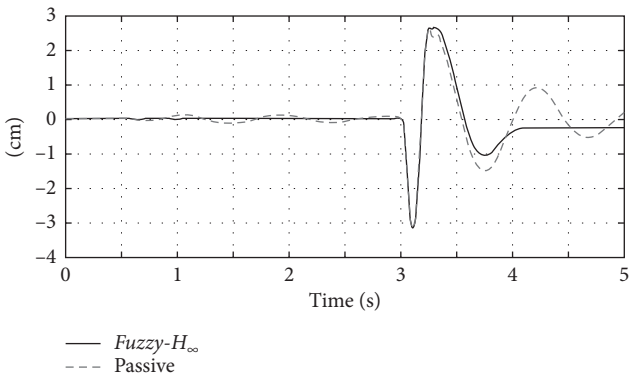

Figure 11: Rear suspension's deflection ($Z_{sr} - Z_{tr}$).

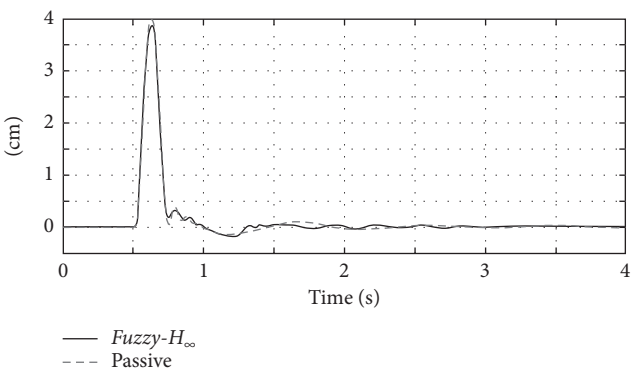

Figure 12: Front tire displacement (Z_{tf}).

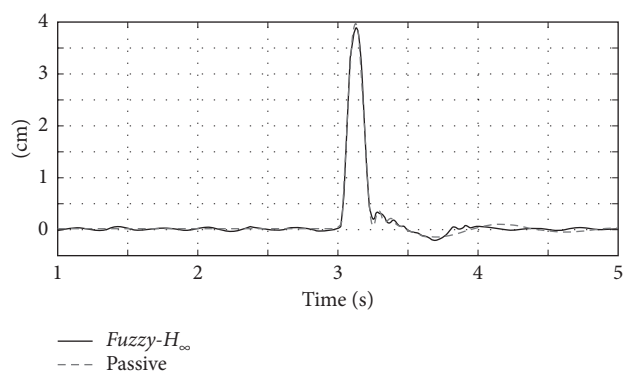

Figure 13: Rear tire displacement (Z_{tr}).

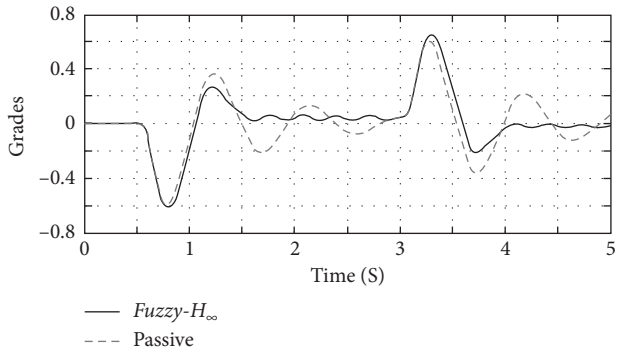

Figure 14: Pitch angle displacement (θ).

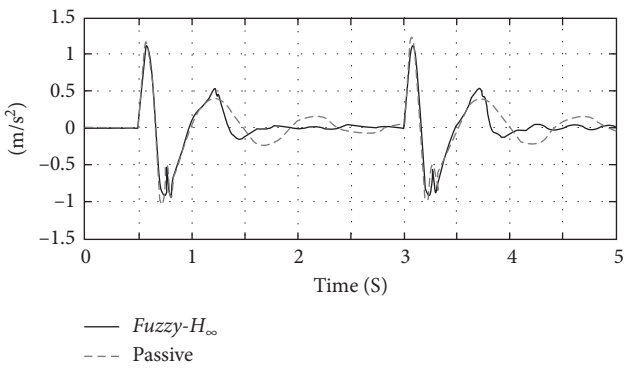

Figure 15: COG chassis acceleration.

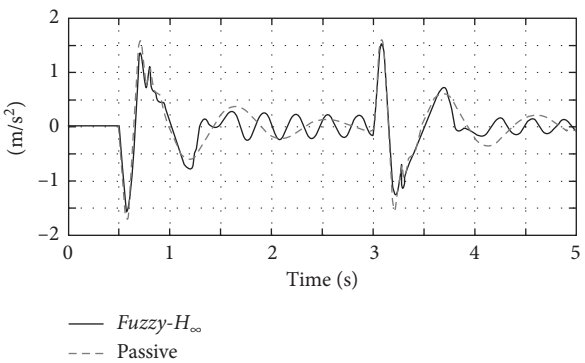

Figure 16: Pitch angle acceleration.

deflections and in *degrees* for the pitch angle displacement. A_{tt} refers to the tire attenuation percentage of the displacement with respect to the road profile. *Val* is the peak acceleration numerical value registered for COG chassis and pitch angle accelerations. Moreover, the settling time (t_s) was compared in quantitative and qualitative manners, depending on whether the steady state was reached in the simulation time or not.

In Table 2, the semiactive suspension improved nine criteria, four indexes had similar results, and three requirements had better results with the passive suspension. Regarding chassis, front and rear suspensions, and pitch suspensions, the improvement was detected at the second transient overshoot and in the settling time as well. About

Table 2: Time domain contrasting for passive and *fuzzy-H_∞* suspensions.

	Z_s		$Z_{sf} - Z_{tf}$		$Z_{sr} - Z_{tr}$		Z_{tf}		Z_{tr}		θ		$\ddot{Z}_s$		$\ddot{\theta}$	
	Max Mp (cm)	t_s (s)	Max Mp (cm)	t_s (s)	Max Mp (cm)	t_s (s)	Max Att (%)	t_s (s)	Max Att (%)	t_s (s)	Max Mp (degrees)	t_s (s)	Max Val (m/s^2)	t_s (s)	Max Val (rad/s^2)	t_s (s)
Passive	1.51	Larger	−3.15	3.9	−3.15	3.9	0.5	1.2	0.7	1.3	0.6	Larger	1.22	Larger	−1.7	Smaller
H_∞	1.37	Smaller	−3.15	1.5	−3.15	1.5	2.5	1.2	2.75	1.3	0.65	Smaller	1.12	Smaller	−1.6	Larger

physical limits, the two suspensions reached the maximum dampers' limits. In addition, both suspensions exhibited a similar performance for tire transmissibility. For COG chassis acceleration, the *fuzzy-H_∞* solution improved the settling time. Finally, pitch angle acceleration for the semiactive proposal performed a drawback in the settling time. In general terms, under the testing conditions established herein, the proposed semiactive suspension in closed loop had a better performance than the passive suspension.

6.2. Comparison with Reported Work. As mentioned in the introduction, other authors have also obtained results that improve the passive suspension performance. Although it is complicated to compare the outcomes of this study with other one because disturbance characteristics and numerical suspension's parameters are different and research efforts focus on different process variables, a modest comparison among recent reported work is accomplished to provide some external validity to this research. From the reported outcomes in the time domain (response to a bump-like disturbance), this inquiry calculated the percentage of achieved improvement with respect to a benchmark passive suspension.

Wang et al. [20] developed an optimized static output feedback controller and reduced by nearly 90% the maximum peak value registered for $\ddot{Z}_s$ and $\ddot{\theta}$. Pang et al. [24] implemented a variable universe fuzzy control with fuzzy neural networks and particle swarm optimization and reduced $\ddot{Z}_s$ and $\ddot{\theta}$ by approximately 39%, whereas suspension deflections (front and rear) were reduced by 33%. In addition, Benariba et al. [49] developed a suspension with sliding mode control supplemented with Lyapunov surfaces and managed to reduce the Z_s and θ by approximately 40%, while the deflection was reduced by 70%. The above results are compared against those obtained herein. A reduction of 10% was achieved for Z_s and θ, and 8% for $\ddot{Z}_s$ and $\ddot{\theta}$. Although the differences between suspension performances are considerable, this study has the advantage of measuring a larger set of process variables in the time domain and including tests in the frequency domain with clearly defined performance indices. It is important to highlight that all performance indexes, time domain and frequency domain, comply with the defined criteria in Section 2.

6.3. Frequency Domain Tests. The signal inputs for frequency-domain simulations were defined in Section 2.2. Frequency results are presented as descriptive functions, also known as pseudo-bodes [50], and they are illustrated in Figures 17–24.

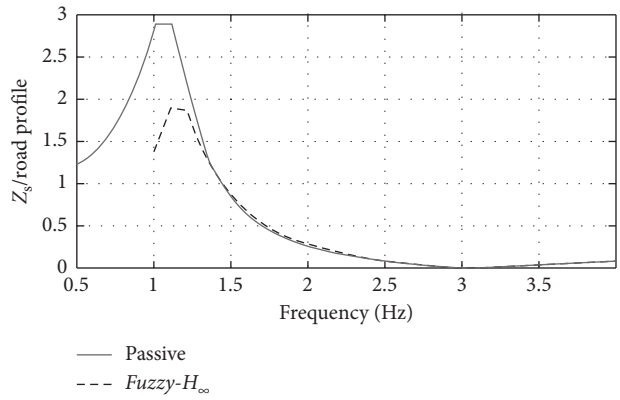

Figure 17: Ratio between chassis displacement and road disturbance.

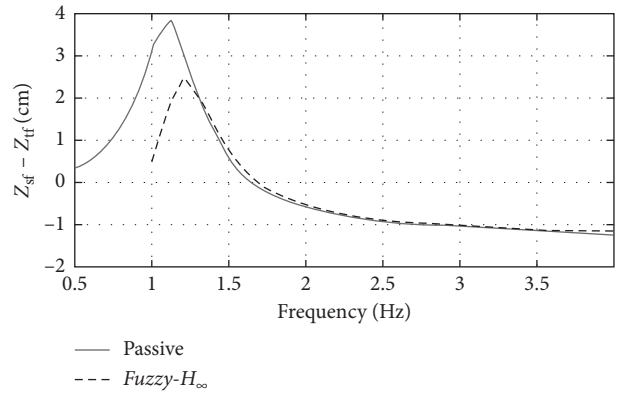

Figure 18: Front suspension deflection (cm).

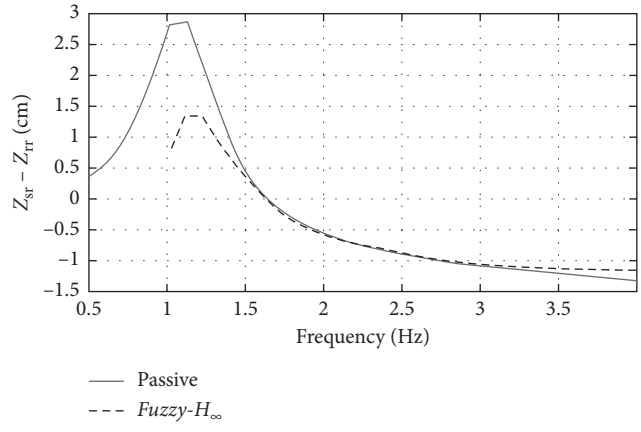

Figure 19: Rear suspension deflection (cm).

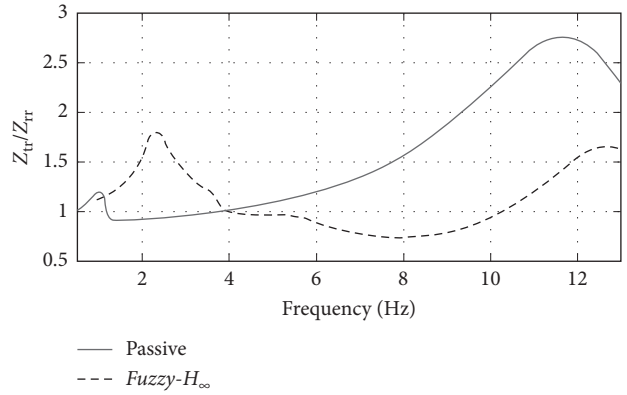

Figure 20: Relation (cm) between front tire displacement and road profile.

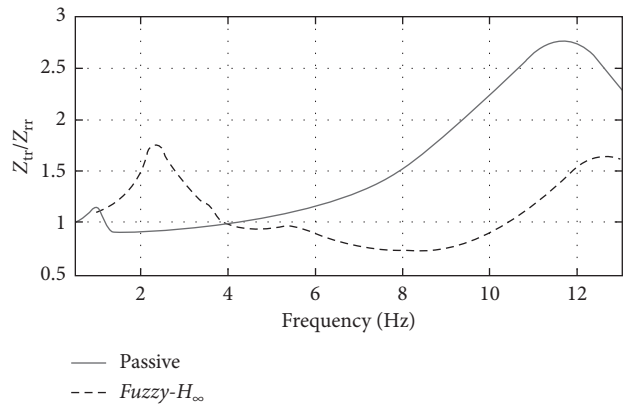

Figure 21: Relation (cm) between rear tire displacement and road profile.

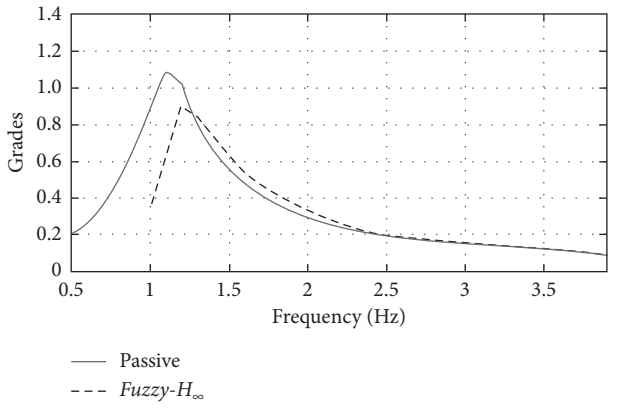

Figure 22: Pitch angle θ (in degrees). The objective is to reduce θ as much as possible.

For suspension deflection, this must be within MR damper's physical limits (±2.5 cm for the MR dampers in this case study) as portrayed in Figures 18 and 19. Distances a and b are measured from the vehicle's COG to the point where the chassis is in contact with the front and rear suspensions, respectively.

The authors did not find a reported maximum or upper boundary value for pitch angle θ to state that a comfort index

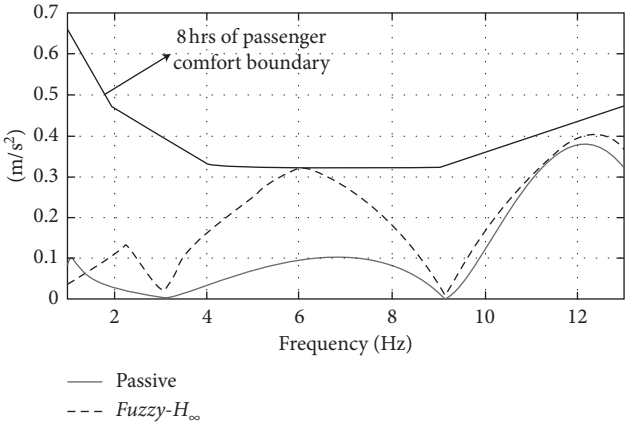

Figure 23: Sprung mass centre-of-gravity acceleration ($\ddot{Z}_s$). The upper wide black line represents the boundary limits to maintain a passenger comfort situation for 8 hrs [28].

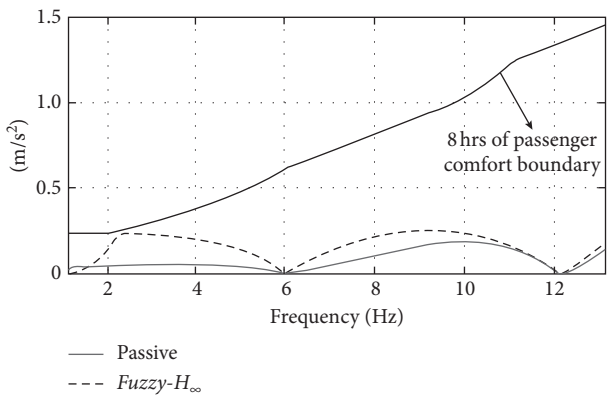

Figure 24: Pitch angle acceleration ($\ddot{\theta}$). The upper wide black line represents the boundary limits to maintain a passenger comfort situation for 8 hrs [28].

is met; however, the objective is to reduce this angle as much as possible to have more stability; i.e., pitch angle magnitude is inversely proportional to stability [31]. Figure 22 depicts the pitch angle for the passive and semiactive suspensions. The maximum pitch angle with the passive suspension is 1.1°, whereas a top angle of 0.9° is obtained with the semiactive suspension. Hence, for the experiment carried out, the semiactive suspension is 18.2% more stable than passive solution.

Figures 23 and 24 portray $\ddot{Z}_s$ and $\ddot{\theta}$. The wide black line indicates a passenger's comfort limit. In the former one, the limit refers to the maximum allowable rms vertical chassis acceleration of the chassis, whereas the latter figure includes rms maximum limit for lateral acceleration over pitch axis. In Figure 24, pitch angle acceleration is expressed in m/s^2, as result of having applied equation (3). Both chassis and pitch angle accelerations are root-mean-square values. If accelerations are maintained below the marked boundary, it can be stated that a passenger's comfort will be preserved for 8 hours as explained in [28].

The results in Figures 17–24 are summarized in Table 3, where the numerical values are the highest possible in the

Table 3: Summary of suspensions performance. Unless indicated, all numerical quantities are in cm.

	Max (Z_s/road profile)	Max (Z_{tf}/Z_{rf})	Max (Z_{tr}/Z_{rr})	Max (Z_{sf}–Z_{tf}), is it within limits?	Max (Z_{sr}–Z_{tr}), is it within limits?	rms $\ddot{Z}_s$ complies with [28]?	θ (degrees)	rms $\ddot{\theta}$ complies with [28]?
Passive	2.89	2.78	2.77	3.8—no	2.9—no	Yes	1.1	Yes
H_∞	1.89	1.77	1.75	2.47—yes	1.36—yes	Yes	0.9	Yes

testing range. Compared with a reference passive suspension, the proposed *fuzzy-H_∞* solution complies with all criteria.

It is worthwhile to remark the defined performance criteria in Section 2 because they help to highlight the relevance of the obtained results. For low frequencies, the passive suspension was not able to keep the (chassis displacement/road profile) relation below 2.0, and it also could not maintain the gain (*tire displacement/road profile*) smaller than 1.8 around the sprung masses' resonance frequencies. In the terms defined by the performance criteria, the chassis was not able to isolate passengers from the road disturbances, nor to guarantee the tires to be always in contact with the floor. The same situation applies for suspension travel at low-frequencies. The passive suspension failed to keep it inside the physical range and this problem reduces the damper's useful life. These three difficulties were solved with the proposed solution.

The suspension with MR dampers improved the performance criteria and physical restriction maximum values in almost all cases, except for the rms $\ddot{Z}_s$ and $\ddot{\theta}$; however, both criteria complied with the comfort criterion reported by Wong [28]. A quantitative comparison between both performances highlights the relevance of the herein outcomes. When comparing the table's first four performance index maximum values, it is observed that *fuzzy-H_∞* improved the performance of the passive suspension between 30% and 35%. Moreover, the pitch angle was enhanced by 18%, and the rear suspension travel was reduced by 53%. The opportunity areas are observed in the rms $\ddot{Z}_s$ and $\ddot{\theta}$, where the passive suspension performed better.

7. Conclusions and Future Work

It is possible to synthesize a competitive *fuzzy-H_∞* controller for a one-half semiactive vehicle suspension with two MR dampers that considers actuator's dynamics and weighted functions during controller design. Due to all nonlinearities in the control design, the design challenge increases due to additional restrictions, but it contributes to more realistic results. To the best of author's knowledge, there is not reported work that considers actuator's dynamics in the controller computation for this type of system.

The proposed control complied with all frequency-domain requirements and increased considerably the passive suspension performance in the time domain Two additional performance criteria, not included in the reviewed work, had been considered. Root mean square vertical and pitch chassis accelerations were measured and compared with benchmarks proposed by the International Organization of Standardization. Although indices of ride comfort at high frequencies were not improved, they were kept below the limit. The developed research work is justifiable due to the enhancement achieved with the obtained semiactive suspension. Moreover, another contribution is the analysis in the disturbance signal phase angle between front and rear tires. This realistic and relevant issue is not mentioned in previous reported work.

This research has some drawbacks. Each time the state vector is sensed, several membership functions are calculated to generate the control signals towards both dampers. This computational load is added to the operations demanded by the parallel distributed compensator (PDC). This could have a negative impact on the implementation stage. Another disadvantage in the complexity is related to controller computation. A 4-DOF suspension with 4 nonlinearities generates 16 linear subsystems and 256 linear matrix inequalities. This is a considerable number of restrictions to satisfy as part of the controller's synthesis.

Currently, authors are exploring modifications to the *fuzzy-H_∞* controller formulation. To improve the performance criteria, an H_2 approach could consider minimal energy aspects. This last strategy requires to deal with greater complexity during controller computation because additional restrictions must be satisfied. In addition, if the control problem is reformulated, γ could pass to the filters' gains to satisfy the set of LMI while keeping its value less than 1.

Another research line is predictive control. If the length of the vehicle is known, and a disturbance affects the front wheel, after certain time, there will also be an impact on the rear wheel. This information could be employed for control purposes based on an estimated prediction for the back suspension.

A third option is the inclusion of roll angle and/or the yaw dynamics. A current one-half vehicle could be complemented with the roll angle analysis, which is related to rollover and steering stability criteria. The authors consider that this research work has potential towards the full-vehicle suspension control, i.e., vertical, pitch, roll, and yaw dynamics.

Finally, to assess the computed controller in a physical testing system would complement these results. A test bed with MR dampers, springs, tires, and the rest of mechanical components would help to detect possible adjustments when moving from an ideal simulation environment towards a more complex scheme with other external variables such as data acquisition, computational cost of the control algorithm, signal filtering, and mechanical couplings, among others. Although the necessary infrastructure for this type of experiments is not available, it could be managed with partners from another educational institution.

Data Availability

The required data used to support the findings of this study are available from the corresponding author upon request.

Conflicts of Interest

The authors declare that they have no conflicts of interest.

Acknowledgments

The authors are grateful to Tecnologico de Monterrey, Escuela de Ingeniería y Ciencias, through the GIEE-Robótica for funding the publication cost of this research.

References

[1] W. Milliken and D. Milliken, *Race Car Vehicle Dynamics*, SAE International, Warrendale, PA, USA, 1995.

[2] T. Butz and O. Von Stryk, "Modelling and simulation of electro- and magnetorheological fluid dampers," *ZAMM Journal of Applied Mathematics and Mechanics*, vol. 82, no. 1, pp. 3–20, 2001.

[3] J. P. Pauwelussen and H. B. Pacejka, *Smart Vehicles*, Swets & Zeitlinger, London, UK, 1995.

[4] B. F. Spencer Jr., S. J. Dyke, M. K. Sain, and J. D. Carlson, "Phenomenological model for magnetorheological dampers," *Journal of Engineering Mechanics*, vol. 123, no. 3, pp. 230–238, 1997.

[5] J. D. Carlson, D. M. Catanzarite, and K. A. St. Clair, "Commercial magneto-rheological fluid devices," *International Journal of Modern Physics B*, vol. 10, no. 23-24, pp. 2857–2865, 1996.

[6] S.-K. Chung and H. B. Shin, "High-voltage power supply for semi-active suspension system with ER-fluid damper," *IEEE Transactions on Vehicular Technology*, vol. 53, no. 1, pp. 206–214, 2004.

[7] K. Worden and G. R. Tomlinson, *Nonlinearity in Structural Dynamics: Detection, Identification and Modelling*, IoP, London, UK, 2001.

[8] A. G. Thompson and B. R. Davis, "Computation of the rms state variables and control forces in a half-car model with preview active suspension using spectral decomposition methods," *Journal of Sound and Vibration*, vol. 285, no. 3, pp. 571–583, 2005.

[9] R. Jazar, *Vehicle Dynamics: Theory and Applications*, Springer, New York, NY, USA, 2008.

[10] M. Yu, X. M. Dong, S. B. Choi, and C. R. Liao, "Human simulated intelligent control of vehicle suspension system with MR dampers," *Journal of Sound and Vibration*, vol. 319, no. 3–5, pp. 753–767, 2009.

[11] G. Pan and F. Fan, "Fuzzy control and simulation of a new semi-active suspension," in *Proceedings of the International Conference on Transportation, Mechanical, and Electrical Engineering (TMEE)*, pp. 2290–2293, Changchun, China, December 2011.

[12] J. Sun and Q. Yang, "Study on improving riding comfort of tipper," in *Proceedings of the Third International Conference on Measuring Technology and Mechatronics Automation*, pp. 484–486, Shangshai, China, January 2011.

[13] W. Sun, H. Gao, and O. Kaynak, "Adaptive backstepping control for active suspension systems with hard constraints," *IEEE/ASME Transactions on Mechatronics*, vol. 18, no. 3, pp. 1072–1079, 2013.

[14] W. Sun, H. Gao, H. Pan, and J. Yu, "Reliability control for uncertain half-car active suspension systems with possible actuator faults," *IET Control Theory & Applications*, vol. 8, no. 9, pp. 746–754, 2013.

[15] P. Krauze and J. Kasprzyk, "FxLMS algorithm with preview for vibration control of a half-car model with magneto-rheological dampers," in *Proceedings of the IEEE/ASME International Conference on Advanced Intelligent Mechatronics*, pp. 518–523, Besacon, France, July 2014.

[16] W. Sun, H. Pan, and H. Gao, "Filter-based adaptive vibration control for active vehicle suspensions with electrohydraulic actuators," *IEEE Transactions on Vehicular Technology*, vol. 65, no. 6, pp. 4619–4626, 2016.

[17] Y. Kong, D. Zhao, B. Yang, T. Shen, H. Li, and K. Han, "Static output feedback control for active suspension using PSO-de/LMI approach," in *Proceedings of the 2012 IEEE International Conference on Mechatronics and Automation*, pp. 366–370, Chengdu, China, August 2012.

[18] P. Li, J. Lam, and K. C. Cheung, "Multi-objective control for active vehicle suspension with wheelbase preview," *Journal of Sound and Vibration*, vol. 333, no. 21, pp. 5269–5282, 2014.

[19] K. Suzuki, T. Toda, G. Chen, and I. Takami, "Robust H_2 control of active suspension -improvement of ride comfort and driving stability," in *Proceedings of the IEEE Conference on Control Applications (CCA). Part of 2015 IEEE Multi-Conference on Systems and Control*, pp. 1951–1956, Sydney, Australia, September 2015.

[20] G. Wang, C. Chen, and S. Yu, "Optimization and static output-feedback control for half-car active suspensions with constrained information," *Journal of Sound and Vibration*, vol. 378, pp. 1–13, 2016.

[21] P. Krauze and J. Kasprzyk, "Comparison of linear and nonlinear feedback control for a half-car model with MR dampers," in *Proceedings of the IEEE 21st International Conference on Methods and Models in Automation and Robotics (MMAR)*, Miedzyzdroje, Poland, August-September 2016.

[22] S. Mahdi, "Chaotic study and chaos control in a half-vehicle model with semi-active suspension using discrete optimal Ott–Grebogi–Yorke method," *Proceedings of the Institution of Mechanical Engineers, Part K: J. Multi-Body Dynamics*, vol. 23, no. 1, pp. 148–155, 2017.

[23] J. Wu and Z. Liu, "Piecewise affine H_∞ control of half-car magneto-rheological suspension systems," *IFAC-PapersOnLine*, vol. 51, no. 31, pp. 967–972, 2018.

[24] H. Pang, F. Liu, and Z. Xu, "Variable universe fuzzy control for vehicle semi-active suspension system with MR damper combining fuzzy neural network and particle swarm optimization," *Neurocomputing*, vol. 306, pp. 130–140, 2018.

[25] L. C. Félix-Herrán, D. Mehdi, J. J. Rodríguez-Ortiz, R. Ramírez-Mendoza, and R. Soto, "Takagi-sugeno fuzzy model of a one-half semiactive vehicle suspension: lateral approach," *Mathematical Problems in Engineering*, vol. 2015, Article ID 396305, 12 pages, 2015.

[26] L. C. Félix-Herrán, D. Mehdi, J. D. J. Rodríguez-Ortiz, R. Soto, and R. Ramírez-Mendoza, "H_∞ control of a suspension with a magnetorheological damper," *International Journal of Control*, vol. 85, no. 8, pp. 1026–1038, 2012.

[27] D. Bastow, G. Howard, and J. Whitehead, *Car Suspension and Handling*, SAE International, Warrendale, PA, USA, 2004.

[28] J. Y. Wong, *Theory of Ground Vehicles*, Wiley, New York, NY, USA, 2001.

[29] D. Sammier, O. Sename, and L. Dugard, "Skyhook and H8 control of semi-active suspensions: some practical

aspects," *Vehicle System Dynamics*, vol. 39, no. 4, pp. 279–308, 2003.
[30] C. Poussot-Vassal, O. Sename, L. Dugard, P. Gáspár, Z. Szabó, and J. Bokor, "A new semi-active suspension control strategy through LPV technique," *Control Engineering Practice*, vol. 16, no. 12, pp. 1519–1534, 2008.
[31] A.-I. Niculescu, D. Dumitriu, and T. Sireteanu, "On vehicles pitch stability increasing," in *Proceedings of the WSEAS International Conference on Mechanics Engineering, Structures, Engineering Geology*, pp. 313–318, Heraklion, Greece, July 2008.
[32] S.-J. Wu, C.-T. Wu, and T.-T. Lee, "Neural-network-based optimal fuzzy control design for half-car active suspension systems," in *Proceedings of the IEEE Intelligent Vehicles Symposium*, pp. 376–381, Las Vegas, NV, USA, June 2005.
[33] N. Karlsson, M. Dahleh, and D. Hrovat, "Nonlinear H_∞ control of active suspensions," in *Proceedings of the American Control Conference*, pp. 3329–3334, Arlington, VA, USA, June 2001.
[34] A. F. D'Souza and V. K. Gang, *Advanced Dynamics: Modeling and Analysis*, Prentice-Hall, Englewood Cliffs, NJ, USA, 1984.
[35] R. Rajamani, *Vehicle Dynamics and Control*, Springer, New York, NY, USA, 2006.
[36] K. Tanaka and H. O. Wang, *Fuzzy Control Systems Design and Analysis*, John Wiley & Sons, New York, NY, USA, 2001.
[37] E. Hecht, *Optics*, Addison-Wesley, Reading, MA, USA, 1987.
[38] R. Serway, *Física*, McGraw-Hill, México City, México, 1997, in Spanish.
[39] W. Assawinchaichote, S. K. Nguang, P. Shi, and E.-K. Boukas, "Fuzzy state-feedback control design for nonlinear systems with -stability constraints: an LMI approach," *Mathematics and Computers in Simulation*, vol. 78, no. 4, pp. 514–531, 2008.
[40] S. Boyd, L. El Ghaoui, E. Feron, and V. Balakrishnan, *Linear Matrix Inequalities in System and Control Theory*, Society for Industrial and Applied Mathematics (SIAM), Philadelphia, PA, USA, 1994.
[41] H. O. Wang, K. Tanaka, and M. F. Griffin, "An approach to fuzzy control of nonlinear systems: stability and design issues," *IEEE Transactions on Fuzzy Systems*, vol. 4, no. 1, pp. 14–23, 1996.
[42] R. W. Beaven, M. T. Wright, and D. R. Seaward, "Weighting function selection in the H_∞ design process," *Control Engineering Practice*, vol. 4, no. 5, pp. 625–633, 1996.
[43] H. Y. Son, S. G. Jeong, J. Y. Choi et al., "A robust controller design for performance improvement of a semi-active suspension systems," in *Proceedings of the IEEE Symposium on Industrial Electronics*, Pusan, South Korea, June 2001.
[44] C. Scherer and S. Weiland, *Linear Matrix Inequalities in Control*, Delft University of Technology and Eindhoven University of Technology, Eindhoven, The Netherlands, 2005.
[45] K. Ogata, *Modern Control Engineering*, Pearson, New York, NY, USA, 2002.
[46] R. L. Williams II and D. A. Lawrence, *Linear State-Space Control Systems*, John Wiley & Sons, Hoboken, NJ, USA, 2007.
[47] T. Sireteanu, D. Stancioiu, and C. W. Stammers, "Modelling of magnetorheological fluid dampers," *Proceedings of the Romanian Academy, Series A*, vol. 2, no. 3, pp. 27–31, 2001.
[48] M. Avesh and R. Srivastava, "Parametric study on the performance of active suspension system for variable passenger size and repeated road bumps," in *Proceedings of the IEEE International Conference on Intelligent Systems and Control*, Coimbatore, India, January 2016.
[49] H. Benariba, L. Baghli, and A. Boumediene, "Vertical displacement sliding mode control of a half-vehicle active suspension," in *Proceedings of the IEEE 5th International Symposium on Environment-Friendly Energies and Applications*, pp. 1–6, Rome, Italy, September 2018.
[50] J.-J. Slotine and W. Li, *Applied Nonlinear Control*, Prentice-Hall, Upper Saddle River, NJ, USA, 1991.